

ADVERSE PRESSURE GRADIENT TURBULENT FLOWS OVER TWO-DIMENSIONAL SQUARE RIBS

Jonathan M. Tsikata and Mark F. Tachie

Department of Mechanical and Manufacturing Engineering

University of Manitoba

E2-327 EITC, 75A Chancellors Circle, Winnipeg, MB. R3T 5V6 Canada

tachiemf@cc.umanitoba.ca

ABSTRACT

A fully developed channel turbulent flow and an adverse pressure gradient (APG) turbulent flow over smooth and rough walls have been studied using a particle image velocimetry (PIV) technique. The rough walls comprised two-dimensional transverse square ribs of height, $k = 3$ and pitch, $p = 2k, 4k$ and $8k$. It was found that APG and wall roughness enhanced turbulence level compared to the fully developed channel flow. A reduction in friction coefficient was observed for the APG flow in contrast to an increase by roughness. Quadrant analysis demonstrated that Q2 and Q4 events occurred more frequently, and contributed more to the production of the Reynolds shear stress than Q1 and Q3 events. Two-point velocity correlations revealed that the inclination and size of the hairpin packets vary with boundary condition and pressure gradient.

INTRODUCTION

Turbulent flows over rough walls are encountered in diverse industrial and environmental applications. In view of their practical importance, numerous studies have been conducted over the past decades to understand the effects of wall roughness on both the velocity and thermal fields in wall-bounded flows. The roughness elements used in previous studies include two-dimensional roughness elements such as transverse square ribs, and three-dimensional roughness elements such as sand grains. Two-dimensional roughness elements are classified into d -type ($p/k < 2$), intermediate type ($p/k = 4$) and k -type ($p/k > 4$) by Perry et al. (1969).

Hanjalic and Launder (1972) performed measurements in channel with an asymmetric boundary condition (i.e., one side of the channel was roughened with k -type square ribs and the opposite side was smooth). They found that the location where the Reynolds shear stress changes sign (y_{wv}) did not coincide with the locations of maximum velocity (y_U). More specifically, it was observed that y_{wv} is closer to the smooth wall than y_U . This finding was corroborated by recent Direct Numerical Simulation (DNS) results reported by Nagano et al. (2004) and Ikeda and Durbin (2007). Recent hot-wire anemometer and DNS data over intermediate type rough wall reported by Burattini et al. (2008), however, indicated that y_U coincided with y_{wv} . A number of studies were also performed in channels with symmetric boundary conditions, i.e., opposite

sides of the channel are roughened with the same roughness elements (Krogstad et al., 2005; Bakken et al., 2005). Unlike the asymmetric boundary conditions, these studies demonstrated that the mean velocity is symmetric about the channel centre.

Turbulent flows over rough walls are also affected by the mean pressure gradient. In contrast to zero pressure gradient (ZPG) and fully developed channel flows, APG flows over rough walls have not been studied in detail. Therefore, the objective of this paper is to study the effects of APG and roughness on the flow characteristics. This objective is achieved by using a PIV system to conduct velocity measurements over ribs in a channel that consists of a parallel section to produce a fully developed flow and a diverging section to produce an APG flows. The ribs were attached to the lower straight wall of the channel at spacing of $p/k = 2, 4$ and 8 . Measurements were also made over a reference smooth wall to facilitate the interpretation of the rough wall data.

EXPERIMENTAL SET-UP

The test channel consisted of an upstream parallel section to produce a fully developed flow and a diverging section to produce an APG flow. The channel was fabricated from 6 mm thick clear acrylic plates and was inserted into the test section of an existing water tunnel which is 2.5 m long, 0.2 m wide and 0.2 m deep. Figure 1 shows a sketch of the test channel with ribs attached to the lower wall. As shown in the figure, the first 1500 mm of the channel (OA) and the last 400 mm of the channel (BC) have straight parallel upper and lower walls. The upper wall of the 600 mm section of the channel (AB) located between these parallel sections diverges linearly from a height of $2h = 55.5$ mm to 96.5 mm at an inclination angle of 4° . The internal width of the channel was $2B = 186$ mm so that the aspect ratio of the channel varies from 3.35 at the inlet parallel section to 1.93 at the end of the diverging section. The streamwise, wall-normal and spanwise directions are along the x, y and z axes, respectively; $x = 0$ at the inlet to the 55.5 mm \times 186 mm section, $y = 0$ at the top plane of the ribs, and $z = 0$ at the mid-span of the channel. Two-dimensional transverse square ribs with nominal height of $k = 3$ mm were used as the roughness elements. The ribs which spanned across the entire width of the channel were secured to the straight lower wall of the test channel with a thin double sided tape at pitch-to-height ratios of $p/k = 2, 4$ and 8 .

The PIV system comprised of an Nd-YAG laser and

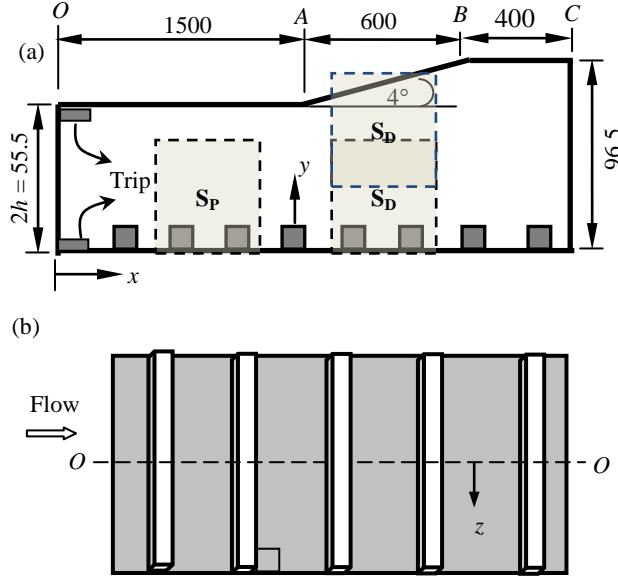


Figure 1. Schematic of side view (a), and plan view (b) of the test section (not to scale). All dimensions in mm.

HiSense 4M camera. The flow was seeded with 10 μm silver coated hollow glass sphere. For each rib configuration, measurements were made in planes located in the upstream parallel section (S_P) and diverging section (S_D). Measurements were also made in a plane channel with no ribs installed, and this boundary condition is the reference smooth wall case. In all cases, measurements were made in the x - y plane at the mid-span of the channel ($z = 0$ mm). The notation R_2S_P is used to represent test condition for $p/k = 2$ in the parallel section and SMS_D represents test condition over the smooth wall in the diverging section. The field of view was approximately 49 mm \times 49 mm in both the parallel and diverging sections. In the diverging section, the lower and the upper boundary layers were measured separately with a similar field of view (Figure 1a). This is necessary to maintain a similar spatial resolution in the upstream parallel section and diverging section. The flow statistics were computed from 6000 instantaneous image pairs using adaptive-correlation with an interrogation area of $\Delta x \times \Delta y = 32 \times 32$ pixels with 50% overlap. The profiles reported in the subsequent sections are spatial averaged results obtained over a pitch. The uncertainty in the mean velocity at 95% confidence level was estimated to be $\pm 2\%$ close to the wall and those for the turbulence intensities and Reynolds shear stress were ± 5 and $\pm 10\%$, respectively of the maximum values. The measurement uncertainty in the estimated friction coefficient, C_f , reported subsequently is $\pm 10\%$.

RESULTS AND DISCUSSION

The test conditions and boundary layer parameters adjacent to the lower smooth and rough walls are summarized in Table 1. In this table, U_m is the spatial averaged maximum

streamwise mean velocity, δ is the boundary layer thickness, θ is momentum thickness, H is the shape factor, $K (= (v/U_m^2)(dU_m/dx))$ is the dimensionless pressure gradient parameter and $Re_\theta (= \theta U_m/\nu)$ is the Reynolds number. Table 1 demonstrates that, irrespective of the pressure gradient, roughness enhanced δ , θ and H compared to the smooth-wall values; and the level of enhancement increased with increasing p/k . As expected, APG reduced U_m but increased δ , θ and H . For $p/k = 8$, the values of δ , θ and H in the diverging section are, respectively, 50%, 68% and 27% larger than the corresponding upstream values. A similar increase in δ and θ by APG was reported by Tachie (2007). The K values indicate a slight acceleration in the parallel section and flow deceleration in the diverging section.

Table 1. Summary of boundary layer characteristics.

Test	p/k	U_m m/s	δ mm	θ mm	H	K $\times 10^{-7}$	Re_θ
SMS_P	–	0.385	24.4	2.0	1.45	1.21	770
SMS_D	–	0.280	37.5	4.9	1.55	–24.49	1370
R_2S_P	2	0.377	26.5	3.3	1.55	1.41	1230
R_2S_D	2	0.313	47.1	7.4	1.95	–23.95	2310
R_4S_P	4	0.394	33.9	4.9	1.84	1.29	1930
R_4S_D	4	0.306	52.4	8.6	2.31	–20.67	2650
R_8S_P	8	0.380	38.4	5.6	1.86	1.93	2120
R_8S_D	8	0.300	57.4	9.4	2.37	–26.59	2820

The mean velocity profiles in outer coordinates are shown in Figure 2a. The present smooth and rough wall results in the parallel section are in good agreement with previous DNS results for fully developed channel flows over a smooth wall (Moser et al., 1999) and k -type ribs (Ikeda and Durbin, 2007). As expected, the profiles over the ribs are less uniform than the smooth wall profiles due to the higher resistance the flow experienced over the ribs. The profiles also become less uniform as p/k increases. Figure 2a also demonstrates that APG makes the U -profile less uniform than the corresponding profiles obtained in the parallel section. This observation can be attributed to an upward spreading of the fluid towards the upper diverging wall and a subsequent deceleration of the flow near the straight lower wall (Shah and Tachie, 2008).

The mean velocity profiles over the ribs are plotted in Figure 2b using the following log-law format employed by Hanjalic and Launder (1972) and Ikeda and Durbin (2007):

$$U^+ = 2.38 \log(y/k) + E \quad (1)$$

The profile over the k -type rib in the parallel section (R_8S_P) is in good agreement with the previous results. As demonstrated in Table 2, the values of E decrease with increasing roughness (or p/k), and also with APG. The profiles over the smooth wall and the ribs are plotted in Figure 2c using the classical log-law:

$$U^+ = 2.44 \ln y^+ + 5 - \Delta B \quad (2)$$

where ΔB is the roughness shift. The present smooth wall data is in good agreement with the DNS data by Moser et al. (1999). The drag characteristics summarized in Table 2 revealed that, irrespective of the mean pressure gradient, the

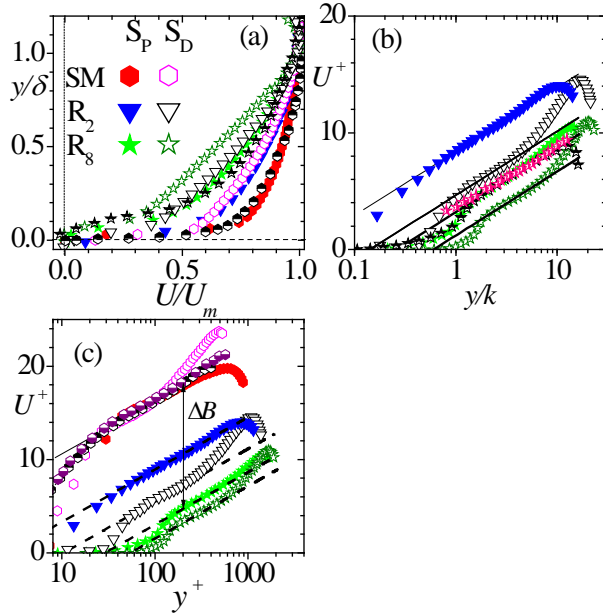


Figure 2. Mean velocity profiles: (a) outer coordinates, (b) and (c) inner coordinates. Symbols: Smooth wall; Moser et al. (1999): \bullet ($Re_\tau = 395$), \circ ($Re_\tau = 590$); k -type: Hanjalic and Launder (1972): \star ; and Ikeda and Durbin (2007): \blackstar .

Table 2. Summary of drag characteristics.

Test	k/δ	U_τ m/s	C_f	E	ΔB	k_s^+
SMS _P	—	0.0195	0.0051	—	0	—
SMS _D	—	0.0118	0.0036	—	0	—
R ₂ S _P	0.113	0.0269	0.0102	8.40	7.5	89
R ₂ S _D	0.064	0.0215	0.0094	4.65	10.8	345
R ₄ S _P	0.089	0.0338	0.0147	4.70	11.6	492
R ₄ S _D	0.057	0.0225	0.0108	2.25	13.1	914
R ₈ S _P	0.078	0.0363	0.0182	3.20	13.1	914
R ₈ S _D	0.052	0.0274	0.0166	1.20	14.8	1799

friction coefficient, C_f increased with increasing p/k . For a given boundary condition, both U_τ and C_f are reduced by APG. This observation is consistent with prior APG results (Perry et al., 1969; Tachie, 2007). The downward shift (ΔB) produced by the rough walls (Figure 2c and Table 2) also increases with increasing p/k and APG. Since the equivalent sand grain roughness, k_s^+ are above the minimum value of $k_s^+ = 70$ suggested for the roughness regime to be fully rough (Schlichting, 1979), all the rib surfaces considered in the present study are in the fully rough regime. Furthermore, APG increased k_s^+ values for a given rib surface by 86% to 288%.

The effects of rib roughness and APG on the streamwise and wall-normal turbulence intensities (u and v), and Reynolds shear stress ($-uv$) are shown in Figure 3a-b. In these plots, the turbulence statistics and wall-normal axis are, respectively, normalized by U_τ and y_{uv} . As noted earlier, y_{uv} corresponds to the y -location where $-uv$ changes sign. In the parallel section, the present data are in good agreement with previous results.

Near the wall ($y = 0.025y_{uv}$), the smooth wall u^+ shows a sharp inner peak, which results from increasing mean strain $\mathcal{Q} = U/\partial y$ as the wall is approached (Figure 3a). The present peak value of 2.6 is identical to the value reported by Bhaganagar et al. (2004). As the roughness effect (or p/k) increases, u_{max}^+ decreases, and its location also shifts further away from the rough wall. The reduction of u^+ near the ribs ($y/y_{uv} < 0.10$) may be attributed to an obstruction of the longitudinal motion of inrushing fluid during the ejection-sweep cycle. This resistance to the longitudinal turbulence motion increases with increasing k_s^+ (Ligrani and Moffat, 1986). Beyond $y/y_{uv} = 0.10$, no distinct roughness effects on u^+ can be observed in the parallel section. The distributions of v^+ and $-u^+v^+$ over SMS_P and R₂S_P are not significantly different. It should be noted that although, $-u^+v^+$ for SMS_P compared well with the DNS data of Moin et al. (1990), the $-u^+v^+$ is low, and this may be due to lack of two-dimensionality of the mean flow. In the inner half of the boundary layer, the distributions of v^+ and $-u^+v^+$ over R₈S_P are substantially higher than the measured values over the smooth wall and d -type rough wall.

In the diverging section, the profiles of u^+ , v^+ and $-u^+v^+$ form a characteristic broad, flat hump in the outer layer. According to Ligrani and Moffat (1986), the broad, flat hump region for u is the region where production of longitudinal turbulence energy is very important (Figure 3a). Grass (1971) argued that the hump in u is due to low momentum fluid entrainment following an inrush stage. The APG data over the smooth wall shows two distinct peaks: one in the inner layer and the other in the outer layer. The inner peak is 3.3 while the outer peak is 2.7. Skåre and Krogstad (1994) also reported an outer peak for their u^2 profile. These peaks are also present in u^+ for R₂S_D. As roughness increases, the inner peak diminished and finally disappeared for R₈S_D. It should be noted that the higher level of u^+ , v^+ and $-u^+v^+$ for SMS_D compared to the corresponding APG data for the rough walls is an indication of enhanced level of turbulence by APG combined with the more rapid decay in U_τ over the smooth wall compared to the rough walls. It is also clear from Figure 3 that u^+ , v^+ and $-u^+v^+$ are noticeably higher in the diverging section than in the parallel section, irrespective of boundary condition. The present results also indicate that for R₂S_P, R₂S_D and SMS_D, y_U occurred closer to the upper smooth wall than y_{uv} . In contrast, y_{uv} occurred closer to the upper smooth wall than y_U for R₈S_P and R₈S_D, which is in agreement with observation by Hanjalic and Launder (1972), and Ikeda and Durbin (2007). The non-coincident of y_{uv} and y_U is an indication that there exist a strong interaction between the rough wall boundary layer and upper smooth wall boundary layer (Hanjalic and Launder, 1972).

The effects of wall roughness and APG on the turbulence motions are also studied using Townsend structure parameter, a_1 . Bradshaw (1967) reported a value of $a_1 = 0.15$ for a turbulent boundary layer, and this is the value adopted in most turbulence models. Because the spanwise component of the velocity fluctuation was not measured in the present study, the following estimate was used: $a_1 = -uv/(1.5(u^2 + v^2))$. Figure 3d demonstrates that, for a given surface, the distribution of

the structure parameter is not significantly modified by APG. Moreover, the data over the smooth wall and d -type ribs are not significantly different. The distributions over the k -type ribs are much higher than the data obtained over the smooth and d -type ribs; in all cases, however, the present values are lower than the typical value of 0.15 reported for a turbulent boundary layer. The lack of APG effects observed in Fig. 3d would imply that APG enhanced the shear and normal stresses proportionately so that their ratio remains nearly constant.

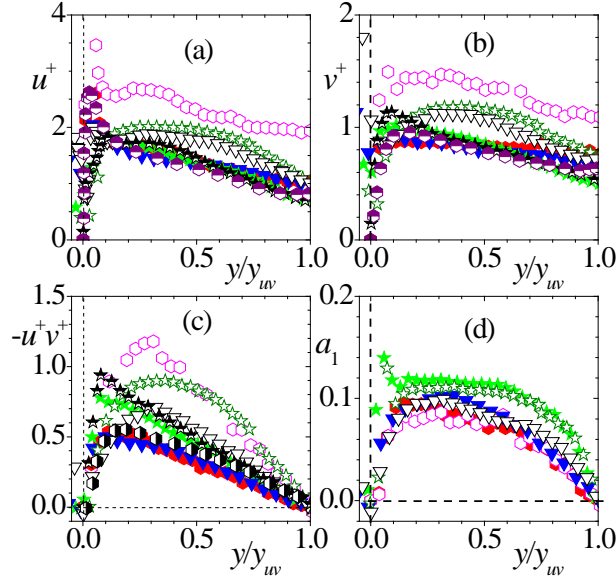


Figure 3. Distribution of (a) streamwise turbulence intensity, (b) wall-normal turbulence intensity, (c) Reynolds shear stress and (d) Townsend structure parameter. Symbols: Present data as in Figure 2. Smooth wall; Moin et al. (1990): \bullet ; Bhaganagar et al. (2004): \circ ; and k -type: Ikeda and Durbin (2007): \star .

Turbulence Structure

The quadrant decomposition is often used to provide insight into the role of coherent structures on the Reynolds-stress producing events. Since $-uv\partial U/\partial y$ is the main contributing term in the turbulence production term, such an analysis will also improve our understanding of the effects of surface roughness and APG on near-wall turbulence production. In this technique, the contribution of the various quadrant events to the overall Reynolds shear stress can be quantified. Following Lu and Willmarth (1973), the overall Reynolds shear at each measurement location is decomposed into the individual contributions from the four quadrants of the u' - v' plane excluding a hyperbolic hole of size H as follows:

$$(u'v')_{i,H} = \frac{1}{N} \sum_{i=1}^N u'v' I_{i,H} \quad (3)$$

where N is the total number of samples and $I_{i,H}$ is an indicator function defined so that

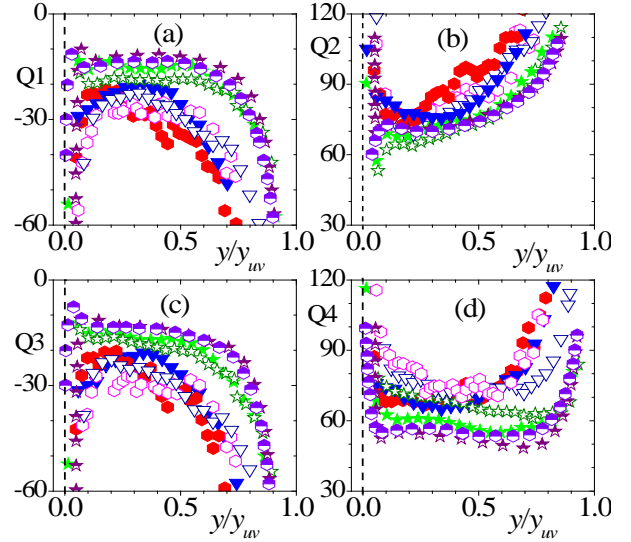


Figure 4. Percentage contribution by the various quadrants. Symbols: Present data as in Figure 2. Krogstad et al. (2005): \circ ; Smooth wall: \bullet ; k -type ribs: \star .

$$I_{i,H}(u',v') = \begin{cases} 1 & \text{if } (u',v') \text{ is in quadrant } i \text{ and if } |u'v'| \geq H \overline{uv} \\ 0 & \text{otherwise} \end{cases} \quad (4)$$

It should be noted that the ejection (Q2) and sweep (Q4) events are the most important events that contribute significantly to $-uv$. The inward (Q3) and outward (Q1) interaction motions, on the other hand, do not contribute to $-uv$. Figure 4 shows the results obtained for the various test condition for $H = 0$. The result for R_{8S_P} is in good agreement with that from Krogstad et al. (2005), but the smooth wall data deviate from the previous smooth wall results. The percentage contribution from Q1 (Figure 4a) and Q3 (Figure 4c) to $-uv$ is always negative, and it increased in the presence of APG. It is also evident that the inward and outward interactions become weaker as roughness increases. The contribution from Q2 is reduced, especially near the wall by APG. Moreover, as roughness effect increases, the Q2 events become less intense. This may be due to trapping of low-momentum fluid between roughness elements, as explained by Grass (1971). The rapid rise in Q2 is due to the transport of low-momentum fluid from the wall region towards the outer region. The contribution from Q4 is stronger near the wall in the presence of APG but as roughness effect increases, the contribution from Q4 diminished. The near-wall spikes in Q4 are likely due to dominant turbulence transport towards the wall.

The two-point velocity correlation function of u' in the x - y plane at a reference point $X_{ref}(x_{ref}, y_{ref})$ separated by ΔX is:

$$R_{uu}(X_{ref}, X) = \frac{u'(x_{ref}, y_{ref})u'(x_{ref} + \Delta x, y_{ref} + \Delta y)}{u(x_{ref} + \Delta x, y_{ref} + \Delta y)u(x_{ref} + \Delta x, y_{ref} + \Delta y)} \quad (5)$$

where u' is the fluctuating velocity, u is the streamwise turbulence intensity. Figure 5 shows contours of two-point correlations of the streamwise fluctuating velocity, R_{uu} centred at $y_{ref}/\delta = 0.4$. The plots are used to quantify the average extent, inclination angle and shape of hairpin packets. In general, the R_{uu} contours are elliptical in shape and elongated in the streamwise direction. The long streamwise correlation in R_{uu} is dominated by elongated low-speed fluid regions within the vortex packets. The streamwise length scale, Lx_{uu} of R_{uu} was estimated as twice the distance from self-correlation peak to the most downstream location on the $R_{uu} = 0.5$ contour (Christensen and Wu, 2005) while the wall-normal length scale, Ly_{uu} of R_{uu} corresponds to the wall-normal distance between the points closest and farthest from the wall on a particular contour level. These length scales as well as the inclination angle for the hairpin packets, β are summarised in Table 3. It is observed that Lx_{uu} decreased in the presence of APG. Krogstad and Skåre (1995) also reported a similar observation and argued that when the flow is subjected to APG, the streamwise vortex stretching becomes less effective. Meanwhile, Ly_{uu} increased with APG. The Lx_{uu} and Ly_{uu} for the smooth wall are larger than those for the d -type rough wall but smaller than those for the k -type rough wall. The inclination angle, β of the hairpin packets varies from 7° to 13° , indicating that the hairpin packets are inclined at relatively shallow angles.

Typical instantaneous velocity fields in the parallel and diverging sections over the smooth wall and k -type ribs are shown in Figure 6. A Galilean decomposition is applied by

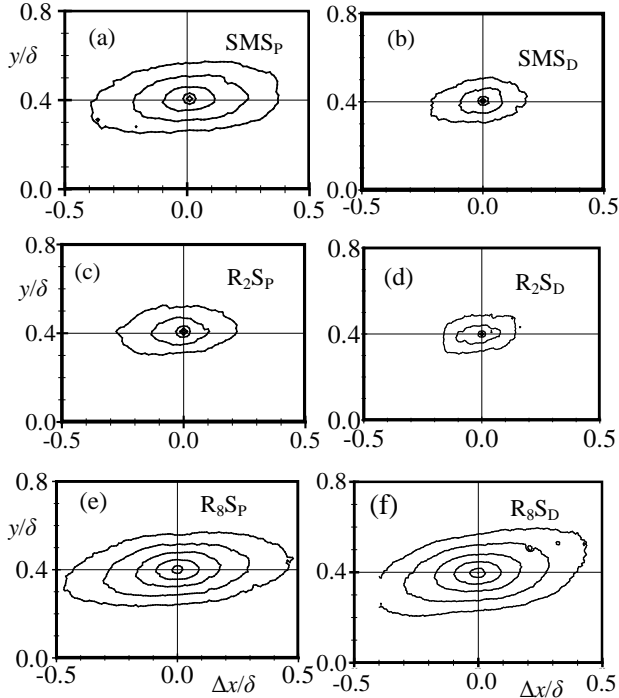


Figure 5. Contours of R_{uu} centred at $y/\delta = 0.4$, outermost contour $R_{uu} = 0.5$, and contour spacing at 0.1.

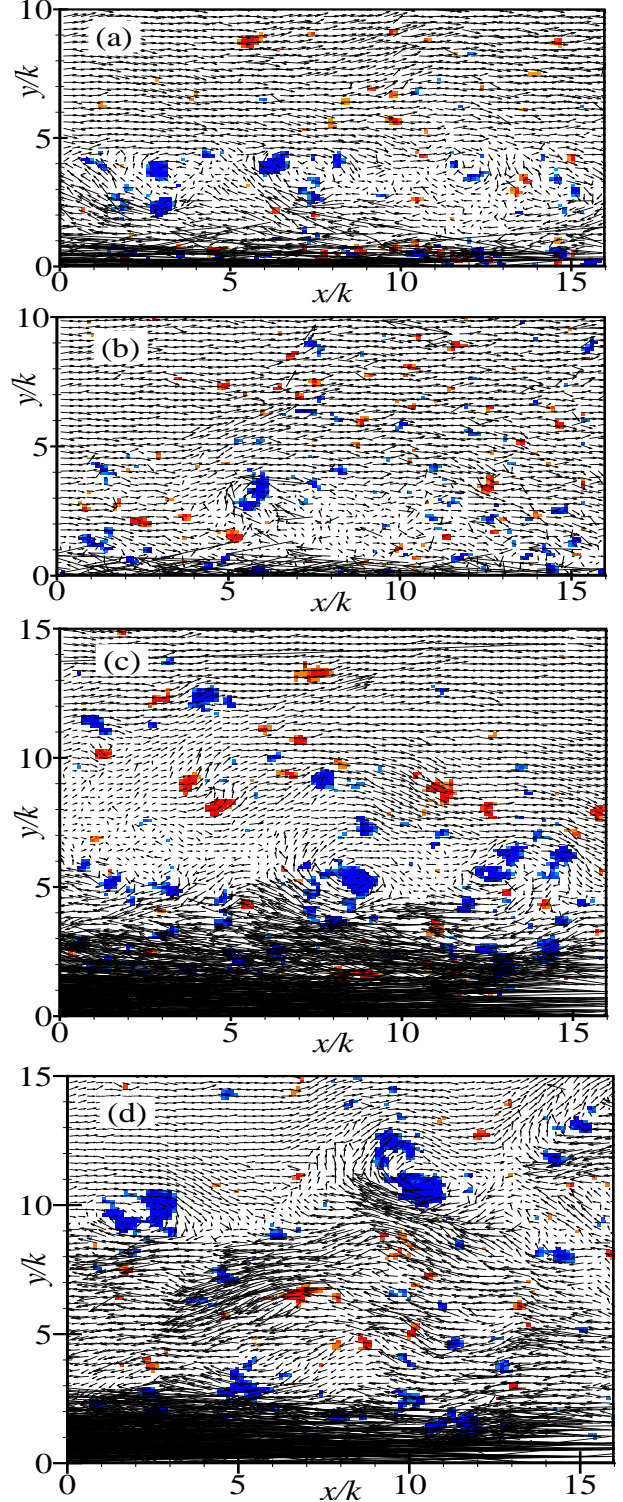


Figure 6. Typical instantaneous velocity field in the x - y plane with contours of swirling strength at the background: (a) SMS_P; $U_c = 0.84U_m$ and (b) SMS_D; $U_c = 0.53U_m$. (c) R₈S_P; $U_c = 0.70U_m$ and (d) R₈S_D; $U_c = 0.72U_m$.

Table 3. Average size and inclination angle of hairpin packets.

Test	β (°)	Lx_{uu}/δ	Ly_{uu}/δ
SMS _P	10.6	0.76	0.33
SMS _D	9.7	0.38	0.20
R ₂ SP	9.1	0.45	0.22
R ₂ SD	9.5	0.33	0.18
R ₄ SP	9.6	0.76	0.28
R ₄ SD	10.5	0.61	0.28
R ₈ SP	7.4	0.93	0.34
R ₈ SD	13.0	0.90	0.39

removing a constant convection velocity, U_c from each field to reveal those vortex structures whose cores are advecting at this particular speed. Contours of swirling strength are also superimposed. The plots show that the velocity fields contain vortex cores that are associated with heads of hairpin vortices. It appears that the vortices in the diverging section are fewer than in the parallel section. The flow fields over the ribs also contain more vortices than over the smooth wall. Over the rough wall, vortices are observed beyond the channel centreline, and these vortices are accompanied by larger scale events similar to the large-scale eruptions of fluid observed by Volino et al. (2009). The large-scale events originate from the ribs, and are likely responsible for the observed differences in the turbulence intensities and shear stress.

SUMMARY AND CONCLUSIONS

A PIV system is used to document the structural features of the flow over smooth and rough walls in a fully developed and APG turbulent channel flows. It was found that roughness as well as APG enhanced turbulence level. Although, APG reduced friction coefficient, a dramatic increase in C_f was observed in the presence of roughness. Quadrant analysis and two-point velocity correlations showed imprints of hairpin packets in the flow. It was found that sweep events are dominant contributors to the Reynolds shear stress in the near-wall region, but away from the ribs ejection contributes significantly to $-uv$. The significant variation of the quadrant events over the various boundary conditions suggests that the effects of roughness persist across most of boundary layer. The R_{uu} demonstrates that there is a long streamwise correlation of low-speed fluid regions in the parallel section compared to the diverging section. However, the wall normal size of R_{uu} increases with APG.

REFERENCES

Bakken, O. M., Krogstad, P.-Å., Ashrafian, A., and Andersson, H. I., 2005, "Reynolds Number Effects in the Outer Layer of the Turbulent Flow in a Channel with Rough Walls", *Physics of Fluids*, Vol. 17, pp. 1-17.

Bhaganagar, K., Kim, J. and Coleman, G., 2004, "Effect of Roughness on Wall-Bounded Turbulence" *Flow, Turbulence and Combustion*, Vol. 72, pp. 463-492.

Bradshaw, P., 1967, "The Turbulent Structure of Equilibrium Turbulent Boundary Layers", *Journal of Fluid Mech.*, Vol. 29, pp. 625-645.

Burattini, P., Leonardi, S., Orlandi, P., and Antonia, R. A., 2008, "Comparison between Experiments and Direct

Numerical Simulations in a Channel Flow with Roughness on one Wall", *Journal of Fluid Mech.*, Vol. 600, pp. 403-426.

Christensen, K. T., and Wu, Y., 2005, "Characteristics of Vortex Organisation in the Outer Layer of Wall Turbulence", *Proceedings, 4th International Symposium on Turbulence and Shear Flow Phenomena*, Williamsburg, Virginia, Vol. 3, pp. 1025-1030.

Grass, A. J., 1971, "Structural Features of Turbulent Flow over Smooth and Rough Boundaries", *Journal of Fluid Mech.*, Vol. 50, pp. 233-255.

Hanjalic, K., and Launder, B. E., 1972, "Fully Developed Asymmetric Flow in a Plane Channel", *Journal of Fluid Mech.*, Vol. 51, pp. 301-335.

Ikeda, T., and Durbin, P., 2007, "Direct Simulations of a Rough-Wall Channel Flow", *Journal of Fluid Mech.*, Vol. 571, pp. 235-263.

Krogstad, P.-Å., Andersson, H. I., Bakken, O. M., and Ashrafian, A., 2005, "An Experimental and Numerical Study of Channel Flow with Rough Walls", *Journal of Fluid Mech.*, Vol. 530, pp. 327-352.

Krogstad, P.-Å., Skåre, P. E., 1995, "Influence of a strong Adverse Pressure Gradient on the Turbulent Structure in a Boundary Layer", *Physics of Fluids*, Vol.7, pp. 2014-2024.

Ligrani, P. M., and Moffat, R. J., 1986, "Structure of Transitionally Rough and Fully Rough Turbulent Boundary Layers", *Journal of Fluid Mech.*, Vol. 162, pp. 69-98.

Moin, P., Shih, T.-H., Driver, D. and Mansour N. N., 1999, "Direct Numerical Simulation of a Three-Dimensional Turbulent Boundary Layer", *Physics of Fluids A*, Vol. 2, pp. 1846-1853.

Moser, R. D., Kim, J. and Mansour N. N., 1999, "Direct Numerical Simulation of Turbulent Channel Flow up to $Re_\tau = 590$ ", *Physics of Fluids*, Vol. 11, pp. 943-945.

Nagano, Y., Hattori, H., and Houra, T., 2004, "DNS of Velocity And Thermal Fields In Turbulent Channel Flow With Transverse-Rib Roughness", *Int. Journal of Heat and Fluid Flow*, Vol. 25, pp. 393-403.

Perry, A.E., Schofield, W. H., and Joubert, P. N., 1969, "Rough Wall Turbulent Boundary Layers", *Journal of Fluid Mech.*, Vol. 37, pp. 383-413.

Schlichting, H., 1979, *Boundary-Layer Theory*" (McGraw-Hill, New York)

Shah, M. K., and Tachie, M. F., 2008, "PIV Study of Turbulent Flow in Asymmetric Converging and Diverging Channels", *ASME Journal of Fluid Engrg.*, Vol. 130, pp.1-15.

Skåre, P. E. and Krogstad, P.-Å., 1994, "A Turbulent Equilibrium Boundary Layer near Separation", *Journal of Fluid Mech.*, Vol. 272, pp. 319-348.

Tachie, M. F., 2007, "Particle Image Velocimetry Study of Turbulent Flow over Transverse Square Ribs in an Asymmetric Diffuser", *Physics of Fluids*, Vol. 19, pp. 1-15.

Volino, R. J., Schultz, M. P., and Flack, K. A., 2009, "Turbulence Structure in a Boundary Layer with Two-Dimensional Roughness", *Journal of Fluid Mech.*, Vol. 635, pp. 75-101.

Lu, S. S., and Willmarth, W. W., 1973, "Measurements of the Structure of the Reynolds Stress in a Turbulent Boundary Layer", *Journal of Fluid Mech.*, Vol. 60, pp. 481-511.